

# Image formation in structured illumination wide-field fluorescence microscopy

Dejan Karadagić<sup>a,\*</sup>, Tony Wilson<sup>b</sup>

<sup>a</sup> *University of Liverpool, School of Biological Sciences, Biosciences Building, Crown Street, Liverpool L69 7ZB, UK*

<sup>b</sup> *University of Oxford, Department of Engineering Science Holder Building, Parks Road, Oxford OX1 3PJ, UK*

Received 24 October 2007; received in revised form 19 January 2008; accepted 19 January 2008

## Abstract

We present a theoretical analysis of the image formation in structured illumination wide-field fluorescence microscopy (SIWFFM). We show that the optically sectioned images obtained with this approach possess the optical sectioning strengths comparable to those obtained with the confocal microscope. We further show that the transfer function behaviour is directly comparable to that of the true confocal instrument. The theoretical considerations are compared with and confirmed by experimental results.

© 2008 Elsevier Ltd. All rights reserved.

*Keywords:* Structured illumination; Optical sectioning; Optical microscopy; Fluorescence microscopy; Wide-field microscopy; Confocal microscopy

## 1. Introduction

The confocal microscope possesses a number of advantages over the conventional optical microscope, and the optical sectioning is arguably the most important one (Wilson and Sheppard, 1984; Wilson, 1990; Pawley, 1995). The traditional construction of a confocal microscope employs a point light source together with a point pinhole detector. It is the presence of the pinhole aperture which is responsible for the optical sectioning since it physically blocks light from out-of-focus planes from reaching the photodetector and hence precludes this light (information) from contributing to the final image. A complete image of the object is built up by scanning. These systems, which are usually built as an ‘add-on’ to a conventional microscope, are very powerful and have found great application in a wide number of fields. They normally require laser light sources since standard microscope illumination systems are usually insufficiently bright. In order to overcome these problems a number of approaches have been taken. Among those there are two developed at the University of Oxford. The first one has concentrated on improving the design of traditional pinhole-based systems (Juškaitis et al.,

1996; Wilson et al., 1996), whereas the second has attempted to modify the conventional optical microscope in such a way as to introduce optical sectioning (Neil et al., 1997). If we define optical sectioning as the requirement that all spatial frequencies within the transfer function attenuate with defocus then it is clear that the conventional microscope does not possess this property. However, if we consider for example the conventional fluorescence case then we find that it is only the zero spatial frequency which does not attenuate with defocus; all the other frequencies are imaged less strongly with increasing defocus. This suggests that if we modify the illumination system in a conventional microscope, so as to project a single spatial frequency fringe pattern onto the object, the microscope will image those parts of the fringe pattern efficiently whose projection onto the object lies within the focal region. We thus obtain an image of the object in which the focal optical section is labelled by a sharply focused grid of lines. Simple processing of three images, taken at three relative spatial positions of the fringe pattern, permits both an optically sectioned and a conventional image to be extracted in real-time. The approach has been demonstrated in both brightfield reflected light imaging (Neil et al., 1997; Wilson et al., 1996) as well as fluorescence (Neil et al., 1998, 2000; Lanni and Wilson, 2000). In this article we theoretically describe the fluorescence case using two methods of obtaining structured illumination: fringe projection and grid projection. In the fringe projection case the structured pattern is formed by the interference of two coherent

\* Corresponding author. Tel.: +44 151 7954508; fax: +44 151 7954431.

E-mail addresses: [dejan@liv.ac.uk](mailto:dejan@liv.ac.uk) (D. Karadagić), [tony.wilson@eng.ox.ac.uk](mailto:tony.wilson@eng.ox.ac.uk) (T. Wilson).

illumination beams, so as to create the appropriate pattern on the specimen. In the grid projection approach the structured pattern is formed by imaging a physical grid object on the specimen.

There have been numerous attempts to exploit structured illumination in microscopy to achieve different goals. Notably, Gustafsson has shown that using basically the same principle as described in this paper it is possible theoretically to improve the lateral resolution of the optical microscope by a factor of two (Gustafsson, 2000). Further, exploiting the nonlinearity properties of fluorophore saturation theoretically an unlimited improvement is possible (Gustafsson, 2005). However, in the reality the improvement is limited by the signal-to-noise ratio and the photobleaching of imaged fluorophores. Bailey et al. (1993) introduce standing wave excitation in the fluorescence microscopy, by which they achieve improved axial resolution. Failla et al. (2003) name this type of microscopy spatially modulated illumination microscopy and claim it can be used for the measurement of the structures with accuracy close to 1 nm. This approach also uses structured illumination, but unlike of the approach described in the paper, its sinusoidal pattern is laid along the illumination axis, which complicates the system setup, and limits its potential applications.

The analysis in this article emphasises the optical sectioning side of the approach, and presents experimental results which confirm that the optically sectioned images of high quality can be achieved by this method.

## 2. Fringe projection—imaging theory

Let us assume the fluorescence specimen, characterised by a spatial distribution of fluorescence  $f(t_1, w_1)$ , Fig. 1, is illuminated with a one-dimensional interference intensity pattern of the form

$$I_{\text{excitation}}(t_1, w_1) = 1 + \mu \cos(\nu t_1 + \phi) \quad (1)$$

where  $\mu$  denotes the modulation depth,  $\nu$  the spatial frequency and  $\phi$  a spatial phase. We have elected to work in optical co-ordinates  $(t, w)$  which are related to real co-ordinates  $(x, y)$  via  $(t, w) = (2\pi/\lambda)(x, y)n \sin \alpha$  where  $n \sin \alpha$  is the numerical

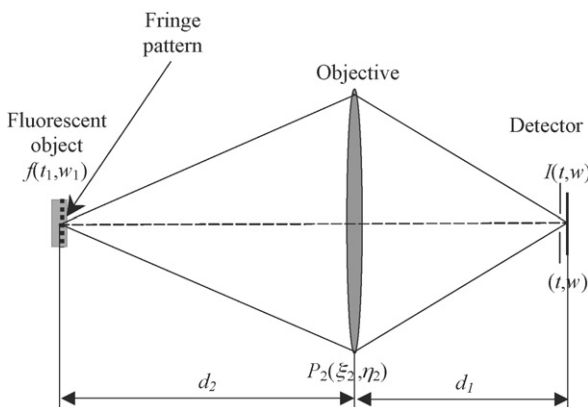


Fig. 1. Schematic diagram of a fringe projection imaging system.

aperture of the objective lens and  $\lambda$  denotes the wavelength. Although the excitation light, used to create interference pattern, may be coherent in nature, the light emitted from the fluorescent specimen is completely incoherent, and given by

$$I_{\text{emission}}(t_1, w_1) = \{1 + \mu \cos(\nu t_1 + \phi)\} f(t_1, w_1) \quad (2)$$

If we now assume that the objective lens has the amplitude point spread function  $h_2$ , and since the final image recorded by the detector in the image plane  $(t, w)$  is equal to the convolution of the emission light and intensity point spread function of the lens (Wilson and Sheppard, 1984), we may write for the intensity of that image

$$I(t, w) = \iint \{1 + \mu \cos(\nu t_1 + \phi)\} f(t_1, w_1) |h_2(t + t_1, w + w_1)|^2 dt_1 dw_1 \quad (3)$$

The excitation and the fluorescence emission wavelengths have also been taken to be equal for simplicity, although in the reality, the emission wavelength must be longer.

Eq. (3) may be written in the following form:

$$I(t, w) = I_0(t, w) + \frac{\mu}{2} \exp(j\phi) I_{\nu}(t, w) + \frac{\mu}{2} \exp(-j\phi) I_{-\nu}(t, w) \quad (4)$$

where

$$I_0(t, w) = \iint f(t_1, w_1) |h_2(t_1 + t, w_1 + w)|^2 dt_1 dw_1 \quad (5)$$

represents a conventional fluorescence image and  $I_{\nu}(t, w)$  is given by

$$I_{\nu}(t, w) = \iint \exp(j\nu t_1) f(t_1, w_1) |h_2(t_1 + t, w_1 + w)|^2 dt_1 dw_1 \quad (6)$$

and we note that  $I_{-\nu}(t, w) = I_{\nu}^*(t, w)$  where the asterisk denotes complex conjugate.

If we now introduce the spectrum of the specimen,  $F(m, n)$  of  $f(t_1, w_1)$ , where  $m$  and  $n$  are spatial frequencies in the  $t_1$  and  $w_1$  directions, respectively, we may recast Eq. (6) as

$$I_{\nu}(t, w) = \exp(-j\nu t) \iint F(m, n) C(m + \nu, n) \exp[-j(mt + nw)] dm dn \quad (7)$$

where the transfer function  $C(m, n)$  is given by the convolution of the pupil functions  $C(m, n) = P(m, n) \otimes P^*(m, n)$  (Wilson and Sheppard, 1984).

Since the function  $C(m, n)$  is also a function of axial distance,  $u$ , we will add that parameter as another argument in the function. The normalised defocus co-ordinate  $u$  is related to the actual defocus,  $z$ , via  $u = (8\pi/\lambda)z \sin^2(\alpha/2)$ .

Eq. (7) now permits us to write an alternative expression for the detected image as

$$\begin{aligned}
 I(t, w; u) = & \int \int F(m, n) C(m, n; u) \exp[-(mt + nw)] dm dn \\
 & + \frac{\mu}{2} \exp(j\phi) \exp(-j\nu t) \int \int F(m, n) C(m + \nu, n; u) \\
 & \times \exp[-j(mt + nw)] dm dn + \frac{\mu}{2} \exp(-j\phi) \exp(j\nu t) \\
 & \times \int \int F(m, n) C(m - \nu, n; u) \\
 & \times \exp[-j(mt + nw)] dm dn \quad (8)
 \end{aligned}$$

We see that the raw image consists of three terms. The first represents a conventional image in which spatial frequencies contained within the passband of  $C(m, n; u)$ , i.e. the region bounded by the circle  $m^2 + n^2 = 4$ , are present—whereas the final two terms represent images with spatial frequency content determined by the regions bounded by the circles  $(m \pm \nu)^2 + n^2 = 4$ . In essence our ‘amplitude’ modulation technique has resulted in a baseband signal (the conventional image) together with two sidebands. The sideband images are also modulated by the spatially varying terms  $\exp(\pm j\nu t)$ .

### 2.1. Extracting the optical sectioning image

In order to show that the image  $I_\nu(t, w; u)$  and its counterpart  $I_{-\nu}(t, w; u)$ , exhibit optical sectioning let us consider the signal  $|I_\nu(t, w; u)|$  detected as a thin fluorescent sheet ( $f(t, w) = 1$ ,  $F(m, n) = \delta(m, n)$ ) is scanned through-focus. From Eq. (7) we can conclude that the response is equal to

$$|I_\nu(t, w; u)| \approx |C(\pm\nu, 0; u)| \quad (9)$$

The axial response is shown in Fig. 2 for variety of values  $\nu$ . The signal is normalised to unity at zero defocus for each value of  $\nu$ . We note that for all values of  $\nu$ , with the exception  $\nu = 0$ , this function exhibits optical sectioning. The strength is determined by the value of  $\nu$ .

Clearly, the  $\nu = 0$  case corresponds to the purely conventional case, and so the optical sectioning disappears as expected.

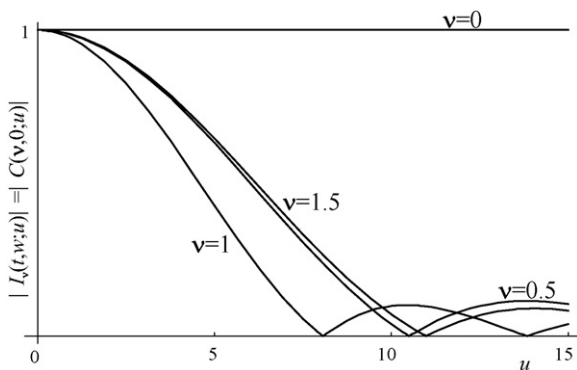


Fig. 2. The axial response to a thin fluorescent sheet,  $|I_\nu(t, w; u)|$  as a function of defocus,  $u$ , for a variety of values of  $\nu$ .

Now the question is—how to extract the image  $|I_\nu(t, w; u)|$  from the raw data? One method would be to record three raw images taken at three equally spaced positions of the fringe pattern. We take the spatial phase  $\phi = \phi_0$  (a constant) at the first position and take an image  $I_1$ . We then move the fringe pattern by one third of a period,  $\phi = \phi_0 + 2\pi/3$ , and take image  $I_2$ . Finally, image  $I_3$  is taken corresponding to  $\phi = \phi_0 + 4\pi/3$ . It is then a simple matter to compute

$$I_1 + I_2 e^{-j2\pi/3} + I_3 e^{j2\pi/3} = \frac{3\mu}{2} \exp(-j\phi_0) I_\nu(t, w; u) \quad (10)$$

and hence

$$|I_\nu(t, w; u)| = |(I_1 + I_2 e^{-j2\pi/3} + I_3 e^{j2\pi/3})| \quad (11)$$

We also note that from the same set of input image we can extract the conventional image

$$\begin{aligned}
 I_0(t, w; u) = & \frac{1}{3}(I_1 + I_2 + I_3) \\
 = & \int \int F(m, n) C(m, n; u) \exp[-j(mt + nw)] dm dn \quad (12)
 \end{aligned}$$

The image  $|I_{\pm\nu}|$  can be calculated either by measuring the values of  $\mu$ ,  $\phi$  and  $\nu$ , and then calculating the final image, or, alternatively using the expression

$$\begin{aligned}
 |I_{\pm\nu}| = & |I_1 + I_2 e^{\mp j2\pi/3} + I_3 e^{\pm j2\pi/3}| \\
 = & \sqrt{\frac{(I_1 - I_2)^2 + (I_1 - I_3)^2 + (I_2 - I_3)^2}{2}} \quad (13)
 \end{aligned}$$

when the actual values of  $\mu$  and  $\nu$  are not required. It is important to stress that the image  $|I_{\pm\nu}|$  does not depend on the depth of modulation,  $\mu$ , although with the increase of  $\mu$  the signal-to-noise ratio rapidly deteriorates (Karadaglić, 2004).

In order to find the optimal value for  $\nu$  to maximise the optical sectioning effect various parameters may be used, and we elect to consider the full width half maximum (FWHM) of the thin fluorescent sheet axial response (Eq. (9)), Fig. 2, as the criterion.

Clearly, the optimal sectioning will be strongest when FWHM is smallest, i.e. we need to solve the equation

$$|C(\nu, 0; u)| = 0.5 \quad (14)$$

for  $\nu$ , so that we have smallest  $u$ .

Since the analytical solution of Eq. (14) is rather difficult, if not impossible, to find we elect to use an approximation for the optical transfer function, due to Stokseth (1969).<sup>1</sup> Thus permits us to write

$$C(\nu, 0; u) = f(\nu) \left\{ 2 \frac{J_1[uv((1-\nu)/2)]}{[uv((1-\nu)/2)]} \right\} \quad (15)$$

<sup>1</sup> The Stokseth approximation is an empirical approximation of experimentally measured optical transfer function (OTF) of a conventional incoherent microscope (Stokseth, 1969).

with  $f(v) = 1 - 0.69v + 0.0076v^2 + 0.043v^3$  where  $J_1(\cdot)$  is a first order Bessel function of the first kind. The maximum sectioning strength is found to corresponds to a normalised spatial frequency  $v = 1$ . At this value of  $v$  the half of FWHM of  $u$  is given by 4.4, which is not substantially larger than the value of 4.0 in the pure confocal case (Wilson, 1990).

We have seen that if we display  $|I_v(t, w; u)|$  we obtain optical sectioning in the same fashion as the confocal microscope. The image of a general object in this case may be written

$$|I_v(t, w; u)| = \left| \iint F(m, n) C(m + v, n; u) + C(m - v, n; u) \exp[-j(mt + nw)] dmdn \right| \quad (16)$$

Unfortunately, this type of microscope is not a linear shift-invariant system, since the transition between  $I_v(t, w; u)$  and  $|I_v(t, w; u)|$  is nonlinear, thus it is not possible to describe the process of obtaining structured illumination wide-field fluorescence microscopy (SIWFFM) image in the terms of optical transfer function for the general case. However in some specific cases, for which we may adopt certain approximations, we may be able to find some effective optical transfer function.

Since the optical transfer function of a conventional microscopy  $C(m, n; u)$  is circularly symmetric let us, for convenience, introduce the transfer function  $g_2$  is equal to

$$g_2(u, \sqrt{m^2 + n^2}) = C(m, n; u) \quad (17)$$

which is plotted in Fig. 3. The index 2 denotes the objective lens.

Let us now consider the imaging of a weak object, for which

$$f(t, w) = 1 + \varepsilon f_1(t_1, w); \quad |\varepsilon| \ll 1 \quad (18)$$

the image may be written as

$$|I_v(t, w; u)| = g_2(u, |v|) + \frac{\varepsilon}{2} \text{Re} \left\{ \iint F_1(m, n) C_{\text{eff}}(m, n; u; v) \times \exp[-j(mt + nw)] dmdn \right\} \quad (19)$$

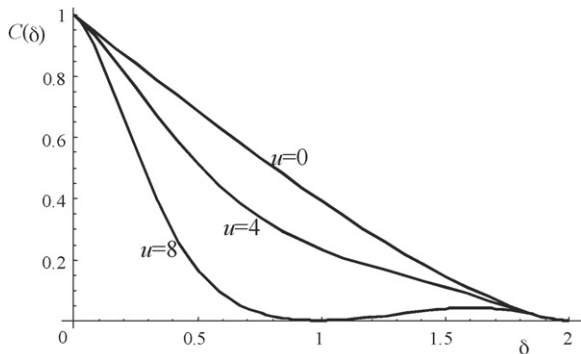


Fig. 3. The form of the optical transfer function  $C(\delta)$ ,  $\delta = \sqrt{\bar{m}^2 + \bar{n}^2}$ , where  $\bar{m} = m\lambda/\sin\alpha$  and  $\bar{n} = n\lambda/\sin\alpha$  represent normalised spatial frequencies, for various values of the defocus  $u$ .

where  $F_1(m, n)$  denotes the Fourier transform of  $f_1(t, w)$  and the effective transfer function  $C_{\text{eff}}(m, n; u; v)$  is given by

$$C_{\text{eff}}(m, n; u; v) = C(m + v, n; u) + C(m - v, n; u) = g_2(u, \sqrt{(m + v)^2 + n^2}) + g_2(u, \sqrt{(m - v)^2 + n^2}) \quad (20)$$

Thus we see that the region of support for  $C_{\text{eff}}(m, n; u; v)$  is given by the overlap of two circles displaced by  $\pm v$  respectively. For the limiting case of  $v = 2$  the cut-off for the  $m$  spatial frequency becomes twice as large as the conventional case and equal to that of the pure confocal case. This observation is the basis of attempts to increase the lateral resolution of conventional fluorescence (Wilson et al., 1998; Heintzmann and Cremer, 1999; Gustafsson, 2000), and standing evanescent wave microscopes (Cragg and So, 2000). Fig. 4 shows the form of  $C_{\text{eff}}(m, 0; u; v)$  for various values of  $v$  illustrating the increase in cut-off with increasing  $v$ . There is, of course, no increase in cut-off for spatial frequencies,  $n$ , in the orthogonal  $w$ -direction. This leads to a distorted region of support for the transfer function as is illustrated in Fig. 5. We note that this distortion may be

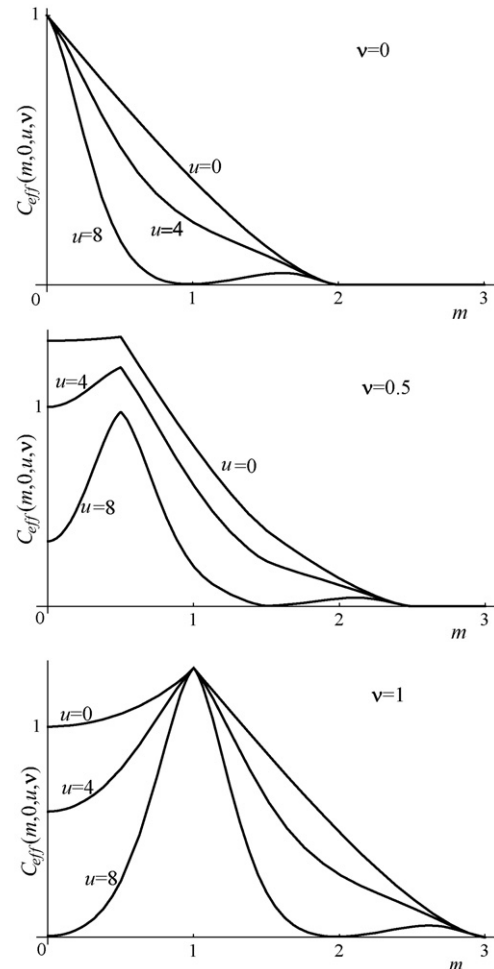


Fig. 4. The form of the effective weak object transfer function  $C_{\text{eff}}(m, 0; u; v)$  in the case of fringe projection for various values of  $v$ . Note the increase in spatial frequency bandwidth from 2 in the conventional case to  $2 + v$  when structured illumination is used.

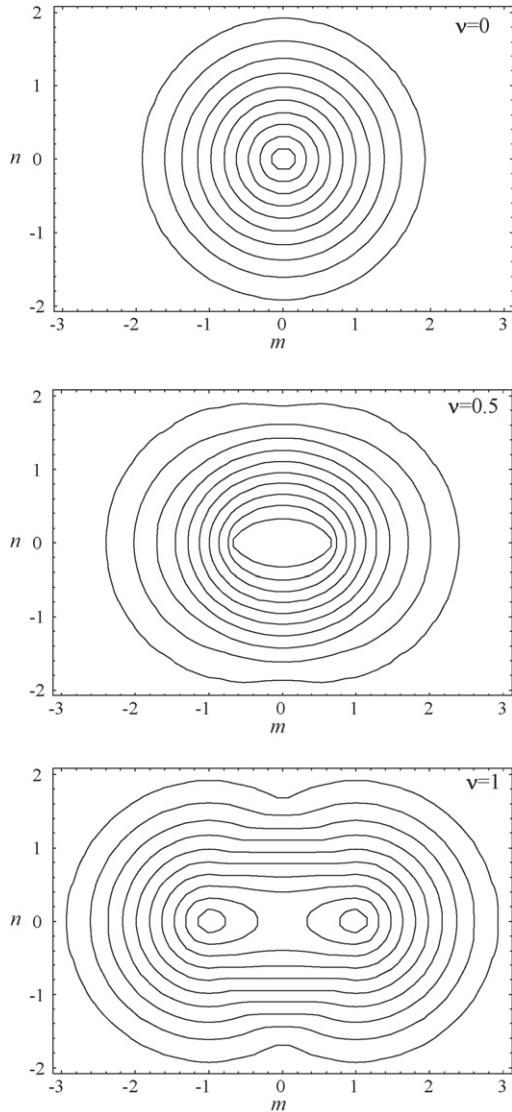


Fig. 5. The transfer function in focus,  $C_{\text{eff}}(m, n; 0; \nu)$  for the cases of  $\nu = 0, 0.5$  and  $1.0$ .

removed to some extent by combining images taken at different orientations of the fringe pattern (Gustafsson, 2005). We shall return to this point later.

Let us now consider the behaviour of the  $C_{\text{eff}}(m, n; u; \nu)$  for the case  $m$  equal to the grid frequency,  $\nu$ , and  $n = 0$

$$C_{\text{eff}}(\nu, 0; u; \nu) = g_2(u, 2\nu) + g_2(u, 0) \quad (21)$$

Since the function  $g_2(u, \delta)$  is equal to 0 for  $\delta \geq 2$ , and  $g_2(u, 0)$  is a constant it is clear that  $C_{\text{eff}}(\nu, 0; u; \nu)$  has different behaviour in the cases  $\nu < 1$  and  $\nu \geq 1$ .

In the case  $\nu < 1$

$$C_{\text{eff}}(\nu, 0; u; \nu) = g_2(u, 2\nu) + \text{const} \quad (22)$$

which is the function which decreases as  $u$  increases, whereas for the case  $\nu \geq 1$   $g_2(u, 2\nu) = 0$ , and hence

$$C_{\text{eff}}(\nu, 0; u; \nu) = \text{const}. \quad (23)$$

which shows that in the case  $\nu \geq 1$  the ‘optical’ sectioning does not occur for frequencies equal to  $\nu$ .

Observing the form of the curves in Fig. 4 we notice that in the case of defocus the features around the frequency  $m = \nu$  show enhancement, which is in some cases very dramatic. We chose to call this, the effect of enhancement of selective spatial frequencies (Karadaglić, 2004). This effect appears in the interaction between the object zeroth spatial frequency and the frequencies close to  $\nu$ . We will show later that this effect does not occur on the case of single point imaging.

### 3. Grid projection

#### 3.1. Theoretical considerations

Let us now turn to the case when a physical grid is used together with an optical system to project an image of the grid onto the specimen (Neil et al., 1997; Wilson et al., 1998; Lanni and Wilson, 2000). In this case, Fig. 6, the intensity of illumination, which illuminates the specimen is given by

$$I(t_1, w_1; u) = \iint S(t_0) |h_1(t_0 + t_1, w_0 + w_1)|^2 dt_0 dw_0 \quad (24)$$

where we have assumed incoherent illumination of the grid, and the transmissivity of the grid is  $S(t_0)$ .

If the transmissivity of the grid is written as  $S(t_0) = 1 + \mu \cos(\nu t_0 + \phi)$  then we can re-write Eq. (24) as

$$I(t_1, w_1; u) = 1 + \mu g_1(u, \nu) \cos(\nu t_1 + \phi) \quad (25)$$

where  $g_1(u, \nu)$  is OTF of the system which images the grid onto the object

$$g_1(u, \nu) = \iint P_1(\xi, \eta; u) P_1^*(\xi - \nu, \eta; u) d\xi d\eta \quad (26)$$

It is now a straightforward exercise to formally replace  $\mu$  by  $\mu g_1(u, \nu)$  in the expressions we have just developed. The major advantage of imaging a physical grid onto the object lies in the fact that the effective modulation of the fringe pattern,  $\mu g_1(u, \nu)$ , attenuates with defocus which may be expected to improve the performance of the system. Indeed the optical sectioning strength, again characterised by the decay in signal as a thin fluorescent sheet is scanned through-focus, is now given by

$$|I(u; \nu)| = |g_1(u, \nu) g_2(u, \nu)| \quad (27)$$

which for the practical case of  $g_1(u, \nu) = g_2(u, \nu)$  is given by

$$|I(u; \nu)| = |g_2^2(u, |\nu|)| \quad (28)$$

which is plotted in Fig. 7 and is seen to be sharper than the corresponding curves in the fringe projection case.

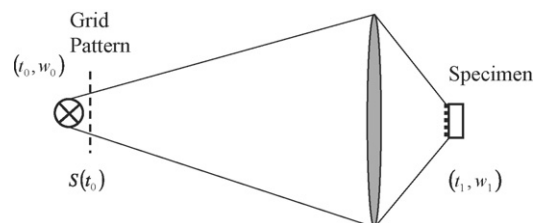


Fig. 6. The basic principle of grid projection SIWFFM.

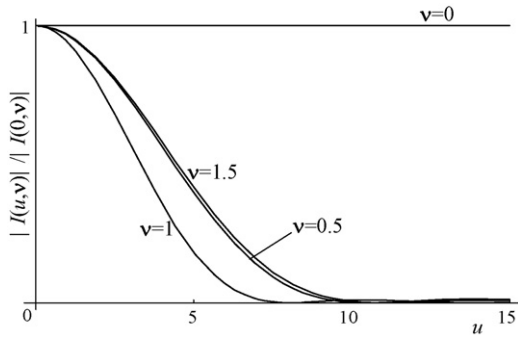


Fig. 7. The axial response to a thin fluorescent sheet,  $I(u, v)/I(0, v)$ , for the grid projection system.

If we compare Figs. 2 and 7 we will find that the half-width of the sectioning curves in this case is roughly  $\sqrt{2}$  smaller than in the fringe projection system.

If we now consider the image of a single point object it is straightforward, using expressions analogous to Eqs. (4) and (6) with the effective modulation  $\mu g_1(u, v)$ , to write this as

$$I(u, v, r) = |I_v(t, w)| = |g_1(u, |v|)||h_2(t, w)|^2 = |g_1(u, |v|)||h_2(r)|^2 \tag{29}$$

where we have introduced the radial co-ordinate  $r = \sqrt{t^2 + w^2}$ . We notice that the image is circularly symmetric and, further and importantly, that the power or the integrated intensity,  $I_{\text{int}}(u)$  (Wilson, 1990):

$$I_{\text{int}}(u) = \int_0^\infty I(u, v, r)rdr \sim |g_1(u, |v|)| \tag{30}$$

decreases with defocus in a fashion analogous to that in a true confocal microscope. We further note that the integrated intensity does not decrease with defocus in the fringe projection case. This is an additional benefit of the grid projection approach.

Finally we note that the effective transfer function is given by

$$C_{\text{eff}}(m, n; u; v) = g_1(u, |v|)[g_2(u, \sqrt{(m+v)^2 + n^2}) + g_2(u, \sqrt{(m-v)^2 + n^2})] \tag{31}$$

The shape of the function  $C_{\text{eff}}(m, 0, u; v)$  is shown in Fig. 8. Compared to Fig. 4 we can see the optical sectioning property is much stronger over whole range of spatial frequencies. Also it can be noted that the effect of the enhancement of selective spatial frequencies is considerably less pronounced, although it is still present.

The function  $C_{\text{eff}}(m, n, u; v)$  exhibits the same asymmetry as that shown in Fig. 5 for the fringe projection case. The asymmetry may be removed to a large extent by combining images taken with the grid rotated by  $60^\circ$  and  $120^\circ$  with respect to the initial position, so that the combined effective function is a sum of the three individual asymmetric functions, describing individual components. In this case  $C_{\text{eff Total}}(m, 0; 0; v)$  takes the

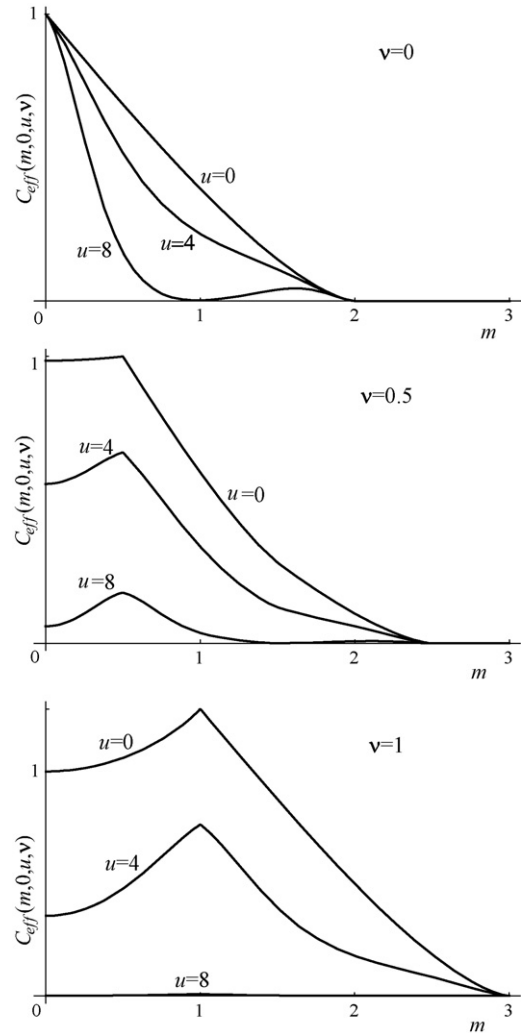


Fig. 8. The form of the effective weak object transfer function  $C_{\text{eff}}(m, 0; u; v)$  in the case of grid projection for various values of  $v$ .

form shown in Fig. 9 where equi-spaced contours have been used.

The form of the transfer function in this case is much more smoothly behaved than in the case when the grid is not rotated. Since optical sectioning is the aim, it is probably best to choose a value of  $v = 1.0$  since this value is optimum in terms of sectioning strength. This corresponds to an enhanced spatial frequency cut-off of  $2 + v = 3.0$ . The cut-off in a true confocal microscope corresponds to  $v = 4.0$  although it is well known (Wilson and Sheppard, 1984; Pawley, 1995) that the transfer function has a very low value for higher spatial frequencies, and the signal from such frequencies is often overwhelmed by noise. This suggests that, although our approach does not have the same actual cut-off as the confocal microscope, it has the capability to behave very similarly in practice. We illustrate this in Fig. 10, where the confocal transfer function is compared with  $C_{\text{eff}}(m, 0; 0; v)$ . Indeed it is arguable that a fringe projection system with  $v = 1.0$  is likely to produce images, which are very comparable, if not superior, to those obtained with confocal microscopes.

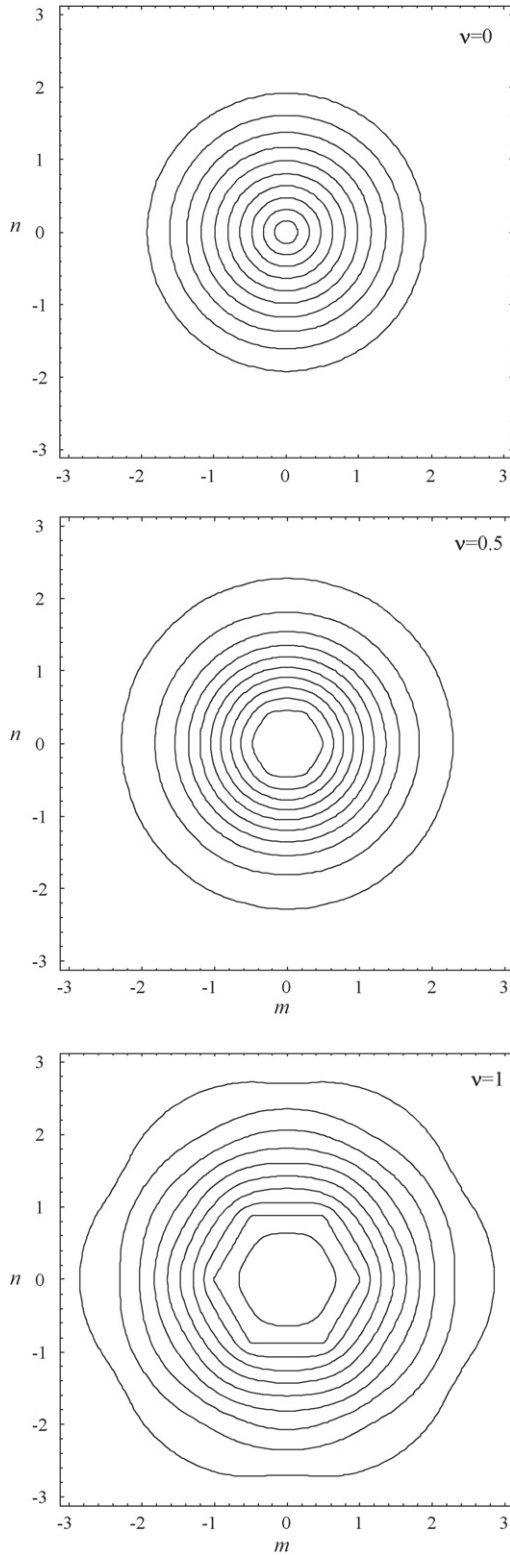


Fig. 9. The transfer function in focus  $C_{\text{eff}}(m, n; 0; \nu)$  for the cases of  $\nu = 0, 0.5$  and  $1.0$ . The transfer function shown is derived from a combination of those representing three orientations of the grid. The contours are drawn at equal spacing between zero and unity.

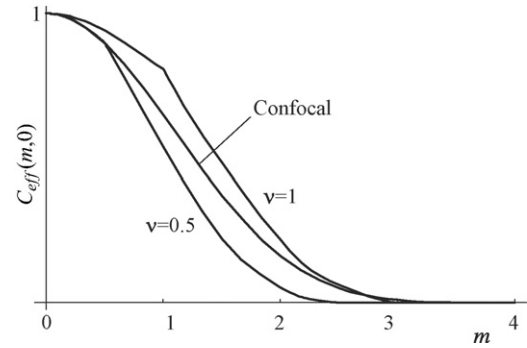


Fig. 10. The transfer function  $C_{\text{eff}}(m, 0; \nu)$  for the cases of  $\nu = 0.5$  and  $1.0$  together with that describing the true confocal fluorescence case.

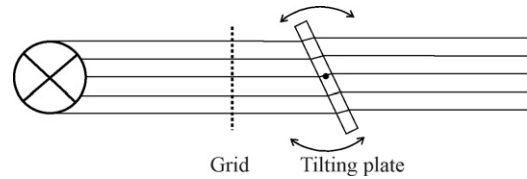


Fig. 11. The principle of obtaining relative phase-shifts in the Zeiss ApoTome system.

### 3.2. Experimental results

In order to demonstrate the abilities of the grid projection microscope we performed a number of experiments using the Zeiss ApoTome system incorporated into an Axio Plan 2 Microscope. This system is based on the grid projection approach described in this paper. Basically the ApoTome system contains a conventional microscope, in our case Zeiss Axio Plan 2, and an accessory, ApoTome slider, which is inserted in the illumination arm of the microscope. The slider contains a physical grid of resolution 25 lines per mm, i.e. of spatial period  $40 \mu\text{m}$ . The grid can be laterally moved so as to be possible to focus on the specimen. In order to obtain the three raw images with different spatial grid positions, the ApoTome slider contains an optical plate, which may be tilted, with a mechanism able to position the angle very precisely (Fig. 11).

We begin by demonstrating the axial response of the system by using a thin fluorescent sheet, consisting of a thin layer of quantum dots.

In the experiment, shown in Fig. 12a the objective used is Zeiss Plan-Neofluar 40x, NA 0.75, and the fluorescence cube Zeiss Filter Set 20, which comprises BP<sup>2</sup> 546/12 nm excitation filter, a 560-nm dichroic beamsplitter and a BP 576–640 nm detection filter. The normalised projected grid frequency was 0.373, which was calculated on the basis of physical measurement of the grid projected and via equation

$$\nu = \frac{\lambda}{T} \frac{1}{n \sin \alpha} \quad (32)$$

<sup>2</sup> BP refers to BandPass filter, in this case it is centred on 546 nm, with BandWidth 12 nm.

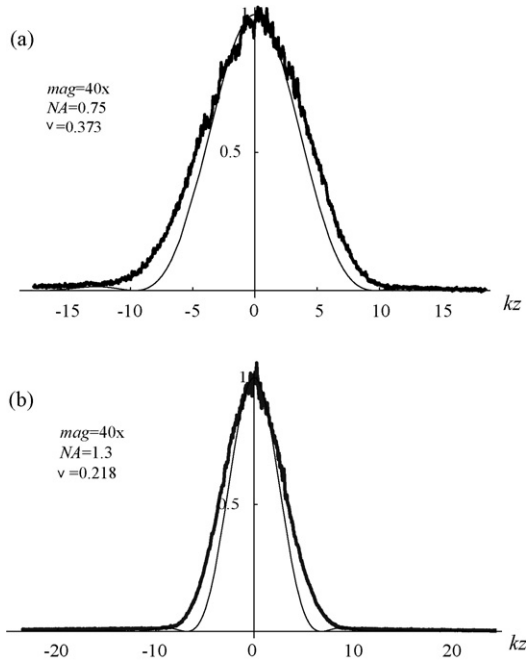


Fig. 12. (a and b) The experimental (thick lines) axial response of microscope, and theoretical predictions (thin lines).

where  $T$  is the spatial period of the grid projected in real units, measured by comparing its size with a calibration target. The thick line in the figure presents the measured axial response. In order to obtain this we took the images when the specimen was slightly tilted, and the thick line is a profile along the slope. In order to compare the experimental results with the theoretical predictions, (Eq. (28)), Fig. 7, we recalculated again the same curves and fitted into the same graph, thin line in Fig. 12. The values of the normalised axial co-ordinate,  $u$ , for the experiment are calculated on the basis of more measurements with different axial positions. Basically we calculated the angle of slope of the tilted sheet by measuring the distance between the peaks of the response curves for different axial positions of the specimen, for which exact values are known, i.e. they are read from the microscope. The experimental and theoretical curves show very good agreement. Of course, there is a slight difference between them, mainly due to the fact that the real fluorescent sample sheet cannot be infinitesimally thin. In Fig. 12b we show the result for the identical experiment, but for the objective lens Zeiss Plan-Neofluar 40x, NA 1.3 (oil). The normalised projected grid pattern frequency in this case is 0.218. Again, very good agreement between the theory and experiment was achieved.

We now move on to obtain image of a pollen grain specimen. The objective used was again Zeiss Plan-Neofluar 40x, NA 1.3 (oil), and the other parameters were the same as in the previous cases. We begin by taking a through-focus stack of image. We took 161 triplets of raw images, with an axial shift of 250 nm between them. In the rows of Fig. 13 we show every 20th image, so the distance between the successive series of images in the figure is 5  $\mu\text{m}$ . In the first column we show one of the three raw images, whereas in the second column of the images the corresponding conventional images are shown. Finally, the third column presents the optically sectioned images. This

figure clearly demonstrates the optical sectioning property, as well as other benefits, such as improved contrast, and crisper image in comparison to the conventional image.

The recorded stack of optically sectioned images can be processed in different ways. Useful information may be obtained, by displaying the data in an extended focus image, shown in Fig. 14.

Another method to display data is via 3D rendering (Fig. 15a–c). In this figure we can clearly see features which are on the back of specimen (higher values of  $z$  co-ordinates, Fig. 15b) on the right-hand side.

In Fig. 16 we show another example from a different type of pollen grain.

#### 4. Discussion

We have shown that the use of structured illumination in a conventional fluorescence microscope results in a raw image consisting of a combination of three partial images. The first,  $I_0$ , represents a conventional image whereas the other two sideband images explore regions of Fourier space bounded by two offset circles  $(m \pm v)^2 + n^2 = 4$ . The offset,  $\pm v$ , caused by the presence of the structured illumination leads to these sideband images exhibiting optical sectioning in the way usually understood in confocal microscopy.

A method has been presented which permits the three partial images to be extracted by suitable processing of the three raw images taken, for example, at three relative spatial positions of the illumination pattern. A very simple method of extracting an optically sectioned image is shown, namely merely displaying  $|I_{\pm v}(t, w; u)|$ . This approach has the advantage that it does not require a detailed knowledge of  $\mu$ ,  $\phi_0$  and  $v$ . However if these parameters are known then they may be removed from the partial images to reveal the following three images, which may be recombined in any desired fashion for final image display.

Rearranging Eq. (5) we may write

$$\begin{aligned} I_0(t, w; u) &= f \otimes |h_2|^2(t, w; u) \\ &= \iint F(m, n) C(m, n; u) \exp[-j(mt + nw)] dmdn \end{aligned} \quad (33)$$

This is, of course, a conventional image. The other two images (Eq. (6)), which may be obtained are given by

$$\begin{aligned} I_v^{(1)}(t, w; u) &= f \otimes \{|h_2|^2 \exp jvt\}(t, w; u) \\ &= \iint F(m, n) C(m + v, n; u) \exp \\ &\quad - j(mt + nw) dmdn \end{aligned} \quad (34)$$

and

$$\begin{aligned} I_v^{(2)}(t, w; u) &= f \otimes \{|h_2|^2 \exp(-jvt)\}(t, w; u) \\ &= \iint F(m, n) C(m - v, n; u) \exp[-j(mt + nw)] dmdn \end{aligned} \quad (35)$$

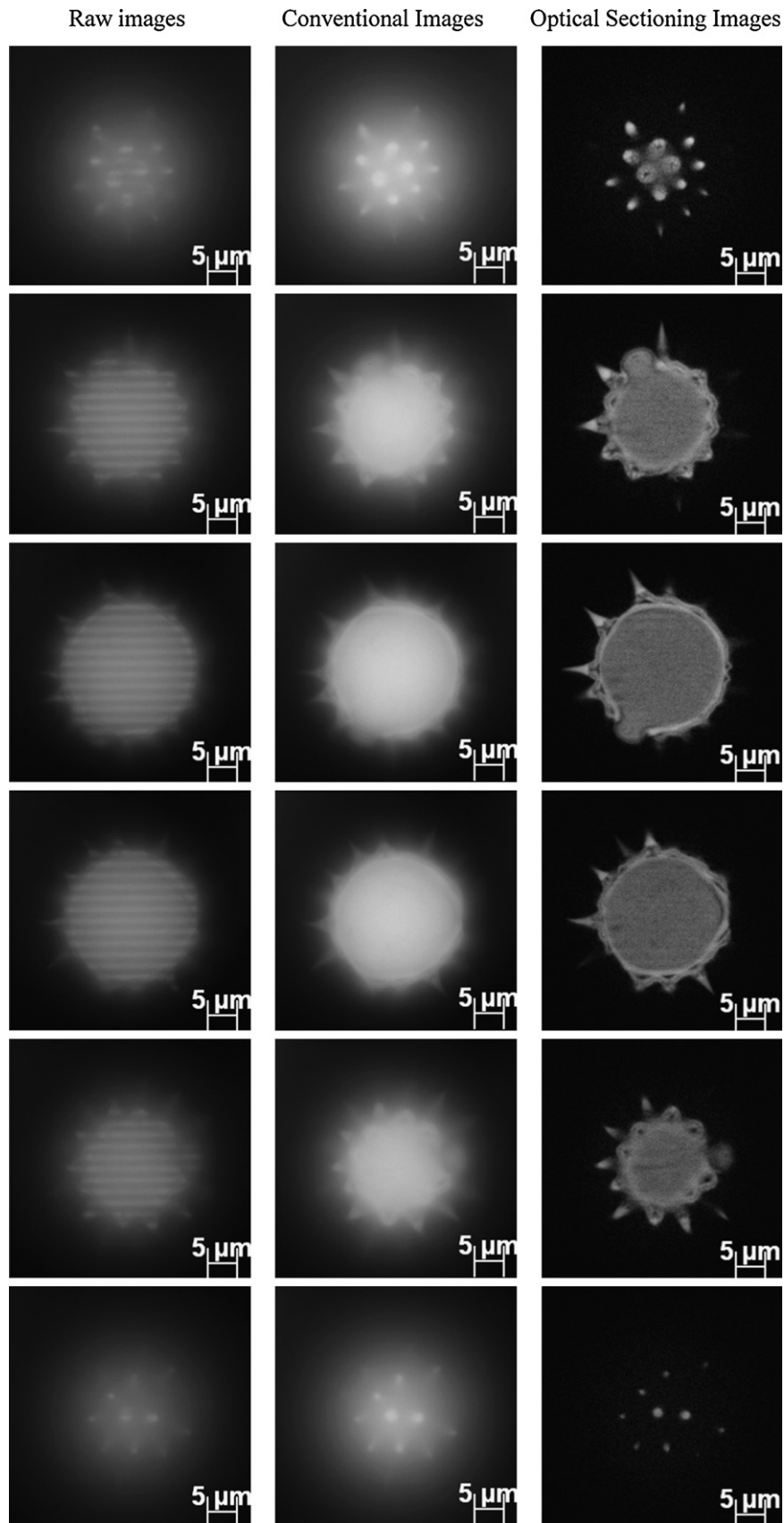


Fig. 13. A through-focus series of images of an autofluorescent pollen grain. The first column shows three raw images, from which the conventional (second column), and the optical sectioning images (third column) are obtained. The axial shift between the successive rows of images is 5  $\mu\text{m}$ .

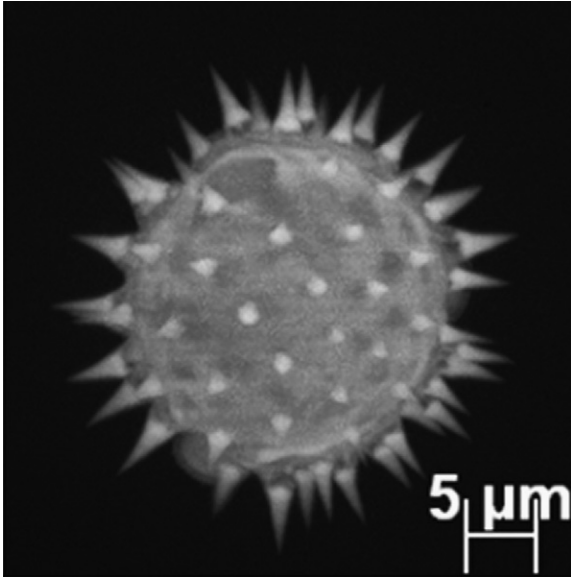


Fig. 14. The extended focus image of a pollen grain.

We can, of course, combine these images in any desired fashion. As an example if we elect to display  $I_v^{(2)}(t, w; u) + I_v^{(1)}(t, w; u)$  we obtain an image with an effective intensity point spread function,  $H(t, w; u)$ , given by

$$H(t, w; u; v) = |h_1|^2(t, w; u) \cos(vt) \quad (36)$$

together with an effective transfer function

$$C_{\text{eff}}(m, n; u; v) = C(m + v, n; u) + C(m - v, n; u) \quad (37)$$

The form of this transfer function has been discussed earlier, Fig. 4, in the case of fringe projection, or corresponding function for the grid projection, Fig. 8. The advantage of this approach is that it is entirely linear shift-invariant, so the transfer function (Eq. (36)) is universal for any kind of specimen. The effective point spread function is modulated by  $\cos(vt)$  and hence, with suitable choice of  $v$ , the point spread function can be sharpened up in the  $t$ -direction. This, of course, leads to an asymmetric image of a single point. However this can be reduced to a large extent by combining images taken at three orientations of the grid pattern as discussed previously.

Another interesting effect may be seen by observing the shape of the transfer function  $C_{\text{eff}}(m, n; u; v)$  in Figs. 4 and 8. Here we see that spatial frequencies close to the frequency of fringe pattern are relatively enhanced, as the specimen moves out of focus. The effect is much more pronounced in the fringe projection case than in grid projection. A similar effect occurs also in brightfield imaging, and it is discussed in more details in Karadaglić (2004).

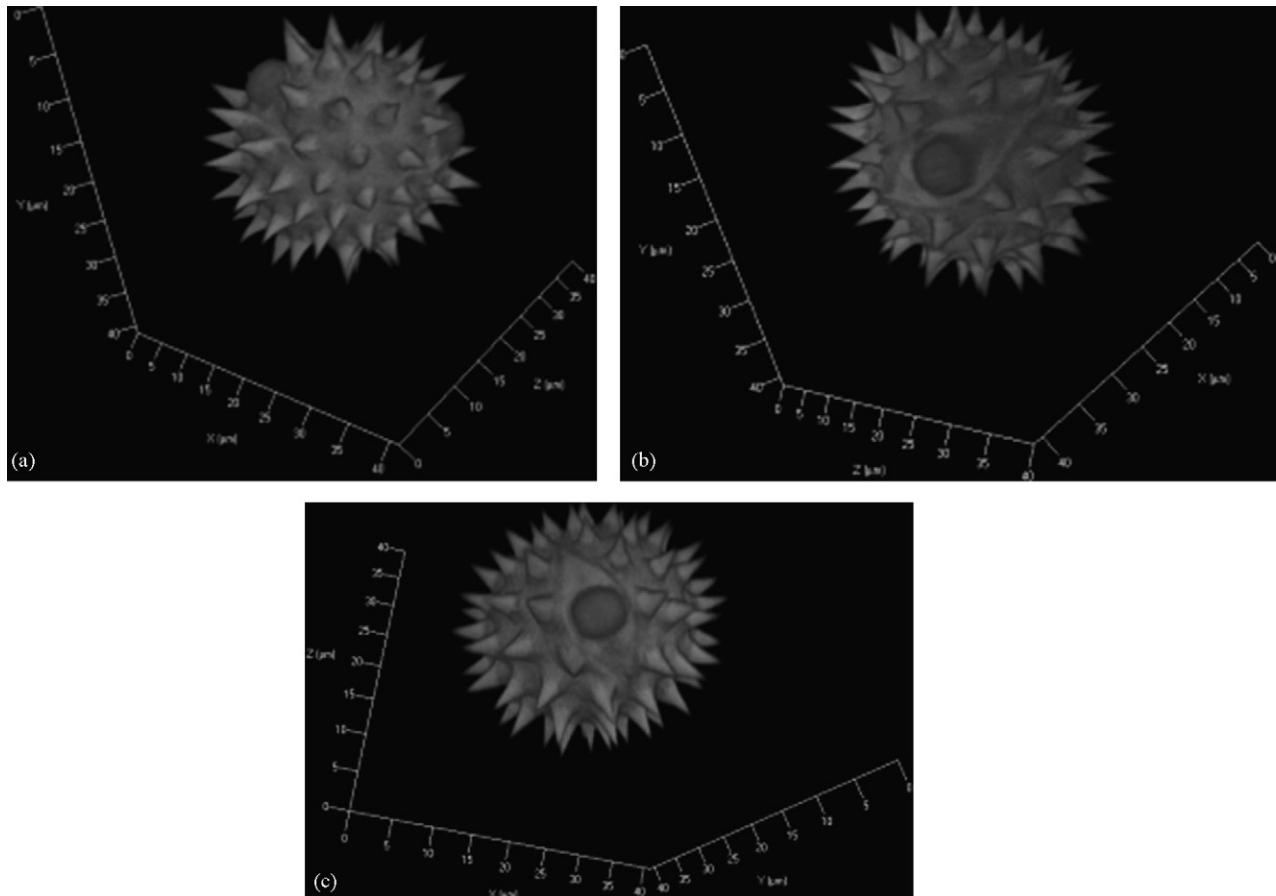


Fig. 15. The “3D image” of the pollen grain specimen observed from three different directions (a–c).

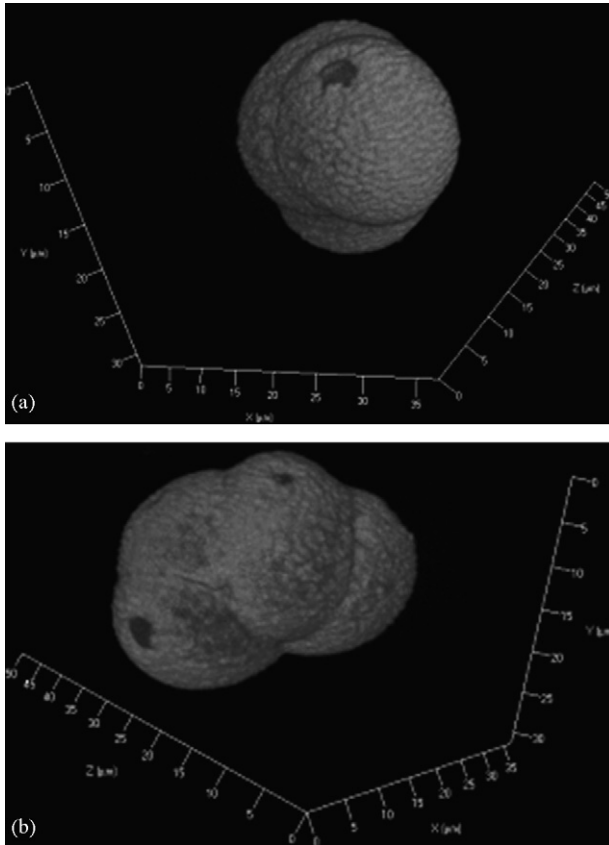


Fig. 16. The “3D image” of another type of pollen grain specimen viewed from two different angles (a and b).

## 5. Conclusion

We have discussed two approaches which permit optically sectioning images to be obtained using conventional fluorescence microscopes employing structured illumination. Both are capable of producing images with optical sectioning strengths comparable to that obtained with true confocal instruments. The grid projection technique also exhibits a decrease in integrated intensity whereas the fringe projection technique does not. The spatial frequency bandwidth is increased in both cases and it was found that good performance, in terms of sectioning and bandwidth, was afforded by choosing a normalised fringe/grid spatial frequency corresponding to  $\nu = 1.0$ . The use of a one-dimensional grid leads in some cases to asymmetric imaging, which may be largely reduced by

combining images taken at three orientations of the grid. The primary method of image display does not require a precise knowledge of the fringe/grid properties. However if these are known then more elaborate postprocessing is possible and images, which are directly comparable to those obtained with true confocal microscopes, may be achieved.

## References

- Bailey, B., Farkas, D.L., Taylor, D.L., Lanni, F., 1993. Enhancement of axial resolution in fluorescence microscopy by standing wave excitation. *Nature* 366, 44–48.
- Cragg, G.E., So, P.T.C., 2000. Lateral resolution enhancement with standing evanescent waves. *Opt. Lett.* 25, 46.
- Failla, A.V., Albrecht, B., Spöri, U., Schweitzer, A., Kroll, A., Hildebrand, G., Bach, M., Cremer, C., 2003. *ComPlexUs* 1 (2) 77–88.
- Gustafsson, M.G.L., 2000. Surpassing the lateral resolution limit by a factor of two using structured illumination microscopy. *J. Microsc.* 198, 82.
- Gustafsson, M.G.L., 2005. Nonlinear structured-illumination microscopy: wide-field fluorescence imaging with theoretically unlimited resolution. *Proc. Natl. Acad. Sci.* 102 (37), 13081–13086.
- Heintzmann, R., Cremer, C., 1999. Laterally modulated excitation microscopy: improvement of resolution by using a diffraction grating. *Proc. SPIE* 3568, 185.
- Juškaitis, R., Wilson, T., Neil, M.A.A., Kozubek, M., 1996. Efficient real-time confocal microscopy with white light sources. *Nature* 383 (6603), 804–806.
- Karadaglić, D., 2004. Wide-field optical sectioning microscopy using structured illumination. DPhil Thesis, University of Oxford.
- Lanni, F., Wilson, T., 2000. *Imaging Neurons: A Laboratory Manual*, vol. 8. Cold Spring Harbor Laboratory Press, p. 1.
- Neil, M.A.A., Juškaitis, R., Wilson, T., 1997. Method of obtaining optical sectioning by using structured light in a conventional microscope. *Opt. Lett.* 22 (24), 1905–1907.
- Neil, M.A.A., Juškaitis, R., Wilson, T., 1998. Real time 3D fluorescence microscopy by two beam interference illumination. *Opt. Commun.* 153, 1–4.
- Neil, M.A.A., Squire, A., Juškaitis, R., Bastiaens, P.I.H., Wilson, T., 2000. Wide-field optically sectioning fluorescence microscopy with laser illumination. *J. Microsc.* 197 (1), 1–4.
- Pawley, J.B. (Ed.), 1995. *Handbook of Biological Confocal Microscopy*. Plenum, New York.
- Stokseth, P.A., 1969. Properties of a defocused optical system. *J. Opt. Soc. Am.* 59, 1314–1321.
- Wilson, T. (Ed.), 1990. *Confocal Microscopy*. Academic Press, London.
- Wilson, T., Sheppard, C.J.R., 1984. *Theory and Practice of Scanning Optical Microscopy*. Academic Press, London.
- Wilson, T., Juškaitis, R., Neil, M.A.A., Kozubek, M., 1996. Confocal microscopy by aperture correlation. *Opt. Lett.* 21 (23), 1879–1881.
- Wilson, T., Neil, M.A.A., Juškaitis, R., 1998. Real-time three-dimensional imaging of macroscopic structures. *J. Microsc.* 191 (2), 116–118.